Journal of Computational and Applied Mathematics 294 (2016) 196–209

Contents lists available at ScienceDirect

Journal of Computational and Applied Mathematics

journal homepage: www.elsevier.com/locate/cam

A new spectral meshless radial point interpolation (SMRPI) method for the two-dimensional Fredholm integral equations on general domains with error analysis

Hedayat Fatahi [a], Jafar Saberi-Nadjafi [a], Elyas Shivanian [b,*]

[a] Department of Applied Mathematics, School of Mathematical Sciences, Ferdowsi University of Mashhad, Mashhad, Iran

[b] Department of Mathematics, Imam Khomeini International University, Qazvin, 34149-16818, Iran

ARTICLE INFO

Article history:
Received 7 February 2015

Keywords:
Spectral meshless radial point interpolation (SMRPI) method
Radial basis function
Fredholm integral equation
General domain

ABSTRACT

In this article, we present a numerical method to solve two-dimensional Fredholm integral equations of the second kind on general domains. The method utilizes meshless and spectral collocation techniques but it is not traditional meshless collocation method. The point interpolation method with the help of strictly positive definite radial basis functions is used to construct shape functions as a basis functions in the frame of spectral collocation methods. These basis functions (shape functions) have Kronecker delta function property. Since the proposed method is meshless, it does not need any domain element and so it is independent of the geometry of the domain. The method reduces the solution of the two-dimensional integral equation to the solution of a linear system of algebraic equations. Convergence analysis with error estimates are given with full discussion. Furthermore, some numerical examples are presented to show the validity and efficiency of SMRPI.

1. Introduction

Consider the following two-dimensional Fredholm integral equation of the second kind

$$u(x,y) = g(x,y) + \lambda \int_{\Omega} K(x,y,t,s)u(t,s)\mathrm{d}t\mathrm{d}s, \quad (x,y) \in \Omega, \tag{1}$$

where g and K are known functions, $u(x,y)$ is the unknown function to be determined, λ is a constant and $\Omega \subseteq \mathbb{R}^2$ is a two-dimensional general domain.

Many problems in engineering and mechanics can be converted into two-dimensional Fredholm integral equations of the second kind. For instance, it is usually required to solve Fredholm integral equations in plasma physics, the image deblurring problem, axisymmetric contact problems for bodies with complex rheology, diffraction theory and the electrochemical behavior of an inlaid microband electrode for the case of equal diffusion coefficients [1]. These types of integral equation also occur as reformulations from some mixed boundary value problems arising in various branches of applied science such as solid and fluid mechanics, electrostatics, heat transfer, diffraction and scattering of waves, etc. [2,3].

There are many works on developing and analyzing numerical methods for solving Fredholm integral equations of the second kind [4–9]. The Galerkin and collocation methods are the two commonly used methods for the numerical solutions

* Corresponding author. Tel.: +98 9126825371.
E-mail address: shivanian@sci.ikiu.ac.ir (E. Shivanian).

http://dx.doi.org/10.1016/j.cam.2015.08.018
0377-0427/

of the two-dimensional integral equations. The analysis for convergence of these methods is well recorded in the literature [4–6]. Han and Wang approximated the two-dimensional Fredholm integral equations by the Galerkin iterative method [10]. Hadizadeh and Asgary solved the linear Volterra–Fredholm integral equations of the second kind by using the bivariate Chebyshev collocation method [11].

Moreover, radial basis functions (RBF) have been used to approximate the solution of one-dimensional integral equations [12]. Golbabai and Seifollahi have applied the one-dimensional RBF networks to solve the linear second kind integral equations of Fredholm and Volterra types [13] and the linear integro-differential equations [14]. A numerical technique based on the spectral method has been presented for the numerical solution of one-dimensional Volterra–Fredholm–Hammerstein integral equations using RBFs in [15]. Golbabai et al. [16] have introduced a numerical method, based on RBFs for the solution of a system of nonlinear integral equations. The numerical solution of two-dimensional Fredholm integral equations of the second kind on the square domain by Gaussian radial basis functions has been introduced in [17]. Also a meshless method based on the moving least squares (MLS) method has been introduced to solve one and two-dimensional integral equations [18]. However, a few number of methods for the solution of the Fredholm integral equations on general domains have been given in the literature [1,18].

In the two last decades, in order to overcome the difficulty of mesh based techniques, so-called meshless methods have been proposed [19–21]. These methods are used to establish system of algebraic equations for the entire domain of the problem without the use of predefined mesh for the domain discretization. There are three types of meshless methods: Meshless methods based on weak forms [22–32], meshless techniques based on collocation techniques (strong forms) [33–35,1,36–38] and meshless techniques based on the combination of weak forms and collocation technique [39–42]. On the other hand, spectral collocation methods (also is called pseudo-spectral method) have been used to solve numerically differential equations by many authors. This method is accomplished successfully by using Chebyshev polynomials approximation and generating approximations for the higher order derivatives through successive differentiation of the approximate solution, the readers are referred to [43–45] (and references therein).

In recent year, a new spectral meshless radial point interpolation (SMRPI) method has been proposed to solve 3-D nonlinear wave equations and two-dimensional diffusion equation with an integral (non-classical) condition [46,47]. In SMRPI, the point interpolation method with the help of radial basis functions is proposed to construct shape functions which have Kronecker delta function property and are used as basis function in the frame of this technique. In this paper, we use this method for solving (1) while the domain of the problem is general. Also, we use strictly positive definite radial basis functions to obtain shape functions without encountering singularity of the moment matrix. To show the efficiency and validity of the present method, we give some numerical experiments.

2. The basis functions in SMRPI

Definition 2.1. A radial basis function $K(x, y) \equiv \phi(x - y) : \mathbb{R}^d \times \mathbb{R}^d \to \mathbb{R}$ is said to be strictly positive definite function if for any set of points $x_1, x_2, \ldots, x_N$ in $\mathbb{R}^d$ the $N \times N$ matrix $A_{ij} = \phi(x_i - x_j)$ is positive definite, i.e.

$$V^T AV = \sum_{i=1}^{N} \sum_{j=1}^{N} v_i v_j A_{ij} > 0$$

for all nonzero $V \in \mathbb{R}^N$ [48].

If $\phi(r)$ be strictly positive definite function on a linear space, then the eigenvalues and determinant of A are positive. Therefore we easily use a linear combination translation of $\phi(r)$ to interpolate data in high dimension [48].

Theorem 2.2 (*Bochner's Theorem [48]*). *Let f be a nonnegative Borel function on $\mathbb{R}$, if $0 < \int_{\mathbb{R}} \varphi < \infty$, then $\hat{\varphi}$ is strictly positive definite, where $\hat{\varphi}$ is the Fourier transform of function φ, which is*

$$\hat{\varphi}(x) = \int_{-\infty}^{\infty} \varphi(y) e^{ixy} dy.$$

Now, one can find many strictly positive definite functions by using this theorem. In Table 1, three important strictly positive definite RBFs are given by using Bochner's Theorem. Consider a continuous function $u(\mathbf{x})$ defined in a domain $\Omega \subset \mathbb{R}^2$, which is represented by a set of field nodes. The $u(\mathbf{x})$ at a point of interest $\mathbf{x}$ is approximated in the form of

$$u(\mathbf{x}) = \sum_{i=1}^{n} R_i(\mathbf{x}) a_i = \mathbf{R}^T(\mathbf{x})\mathbf{a}, \tag{2}$$

where $R_i(\mathbf{x})$ is a strictly positive definite radial basis function (RBF), n is the number of RBFs and coefficients a_i are unknown which should be determined. There are a number of types of strictly positive definite RBFs, and the characteristics of them have been widely investigated [33,49,50]. In the present work, we use those listed in Table 1. In the radial basis function $R_i(\mathbf{x})$, the variable is only the distance between the point of interest $\mathbf{x} = (x, y)$ and a node at $\mathbf{x}_i = (x_i, y_i)$, i.e.

Table 1
Some strictly positive definite RBFs.

Inverse quadratic (IQ)	$\frac{1}{1+(cr)^2}$
Inverse Multiquadratic (IMQ)	$\frac{1}{\sqrt{1+(cr)^2}}$
Gaussian (GA)	e^{-cr^2}

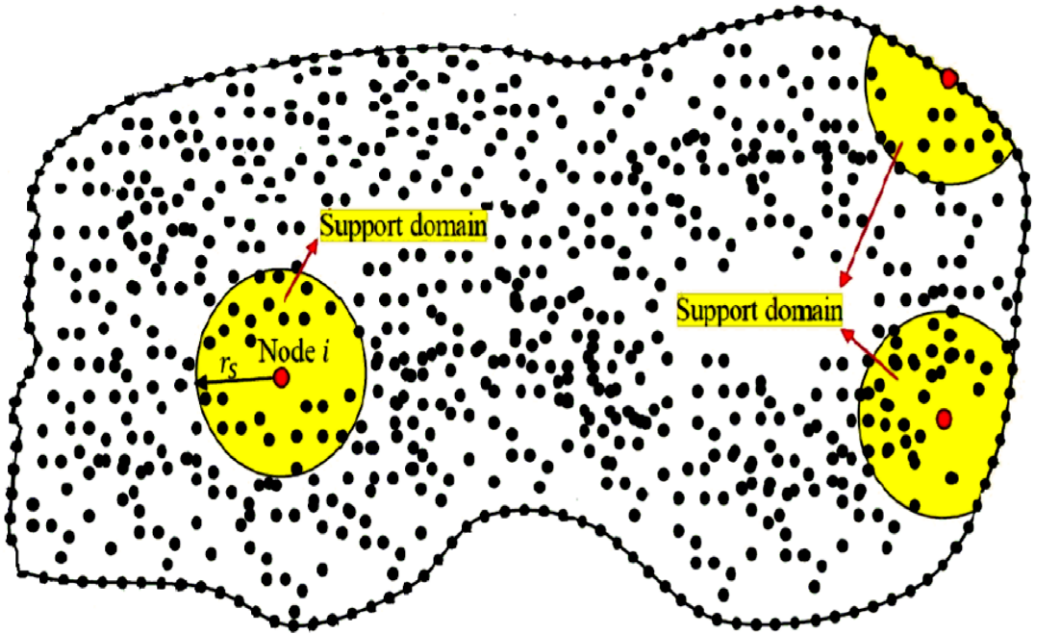

Fig. 1. Local support domains for an arbitrary nodal point $\mathbf{x}_i$ for two-dimensional hypothesis domain.

$r = \sqrt{(x - x_i)^2 + (y - y_i)^2}$. In order to determine a_i's in Eq. (2), a support domain is formed for the point of interest at $\mathbf{x}$, and n field nodes are included in the support domain (see Fig. 1) (support domain is usually a disk with radius r_s). Coefficients a_i in Eq. (2) can be determined by enforcing Eq. (2) to be satisfied at these n nodes surrounding the point of interest $\mathbf{x}$. This leads to the linear system of n algebraic equations, one for each node. The matrix form of these equations can be expressed as:

$$\mathbf{U}_s = \mathbf{R}_n \mathbf{a}, \tag{3}$$

where the vector of function values $\mathbf{U}_s$ is

$$\mathbf{U}_s = \{u_1\ u_2\ u_3\ \ldots\ u_n\}^T, \tag{4}$$

the moment matrix is

$$\mathbf{R}_n = \begin{pmatrix} R_1(r_1) & R_2(r_1) & \cdots & R_n(r_1) \\ R_1(r_2) & R_2(r_2) & \cdots & R_n(r_2) \\ \vdots & \vdots & \ddots & \vdots \\ R_1(r_n) & R_2(r_n) & \cdots & R_n(r_n) \end{pmatrix}_{n\times n}. \tag{5}$$

Also, the vector of unknown coefficients is

$$\mathbf{a}^T = \{a_1\ a_2\ \ldots\ a_n\}. \tag{6}$$

We notify that in Eq. (5), r_k in $R_i(r_k)$ is defined as

$$r_k = \sqrt{(x_k - x_i)^2 + (y_k - y_i)^2}. \tag{7}$$

Since the matrix $\mathbf{R}_n$ is symmetric positive definite, Eq. (3) yields

$$\mathbf{a} = \mathbf{R}_n^{-1}\mathbf{U}_s. \tag{8}$$

Now using Eq. (8), Eq. (2) can be rewritten as

$$u(\mathbf{x}) = \mathbf{R}^T(\mathbf{x})\mathbf{R}_n^{-1}\mathbf{U}_s = \mathbf{\Phi}^T(\mathbf{x})\mathbf{U}_s, \tag{9}$$

where $\mathbf{\Phi}^T(\mathbf{x})$ can be rewritten as

$$\mathbf{\Phi}^T(\mathbf{x}) = \mathbf{R}^T(\mathbf{x})\mathbf{R}_n^{-1} = \{\phi_1(\mathbf{x})\ \phi_2(\mathbf{x})\ \ldots\ \phi_n(\mathbf{x})\}. \tag{10}$$

These n functions of the above vector function are called the RPIM shape functions corresponding to the nodal displacements, then Eq. (9) is converted to the following one

$$u(\mathbf{x}) = \mathbf{\Phi}^T(\mathbf{x})\mathbf{U}_s = \sum_{i=1}^{n} \phi_i(\mathbf{x})u_i. \tag{11}$$

We add the RPIM shape functions which have the Kronecker delta function property, that is

$$\phi_i(\mathbf{x}_j) = \begin{cases} 1, & i = j,\ j = 1, 2, \ldots, n, \\ 0, & i \neq j,\ i, j = 1, 2, \ldots, n. \end{cases} \tag{12}$$

This is because the RPIM shape functions are created to pass thorough nodal values. Moreover, the shape functions are the partitions of unity, i.e.

$$\sum_{i=1}^{n} \phi_i(\mathbf{x}) = 1. \tag{13}$$

3. Discretizing the two-dimensional Fredholm integral equations

Suppose that the number of total nodes covering Ω is N. As we know, n depends on point of interest $\mathbf{x}$ (so, after that we call it $n_{\mathbf{x}}$) in Eq. (11) which is the number of nodes included in support domain $\Omega_{\mathbf{x}}$ corresponding to the point of interest $\mathbf{x}$ (for example $\Omega_{\mathbf{x}}$ can be a disk centered at $\mathbf{x}$ with radius r_s). Therefore, we have $n_{\mathbf{x}} \leq N$ and Eq. (11) can be modified as

$$u(\mathbf{x}) \approx \mathbf{\Phi}^T(\mathbf{x})\mathbf{U}_s = \sum_{j=1}^{N} \phi_j(\mathbf{x})u_j. \tag{14}$$

In fact, corresponding to node $\mathbf{x}_j$ there is a shape function $\phi_j(\mathbf{x}),\ j = 1, 2, 3, \ldots, N$, we define $\Omega_{\mathbf{x}}^c = \left\{\mathbf{x}_j : \mathbf{x}_j \notin \Omega_{\mathbf{x}}\right\}$, then it is clear from the previous section that

$$\forall \mathbf{x}_j \in \Omega_{\mathbf{x}}^c : \phi_j(\mathbf{x}) = 0. \tag{15}$$

The derivatives and integrals of $u(\mathbf{x})$ are easily obtained as

$$\frac{\partial u(\mathbf{x})}{\partial x} = \sum_{j=1}^{N} \frac{\partial \phi_j(\mathbf{x})}{\partial x}u_j, \qquad \frac{\partial u(\mathbf{x})}{\partial y} = \sum_{j=1}^{N} \frac{\partial \phi_j(\mathbf{x})}{\partial y}u_j, \qquad \int_{\Omega} u(\mathbf{x})\mathrm{d}\Omega = \sum_{j=1}^{N} u_j \int_{\Omega} \phi_j(\mathbf{x})\mathrm{d}\Omega. \tag{16}$$

Therefore, the proposed method could be easily applied on the differential equations, integral equations and combination of both.

Now, we consider integral equation (1) and explain how to implement spectral meshless radial point interpolation (SMRPI) method to obtain discrete equations. Substituting approximation expression (14) with $\mathbf{x} = (x, y)$ into Eq. (1) yields:

$$\begin{aligned} \sum_{j=1}^{N} \phi_j(x, y)u_j &= g(x, y) + \lambda \int_{\Omega} K(x, y, t, s) \sum_{j=1}^{N} \phi_j(t, s)u_j \mathrm{d}t\mathrm{d}s \\ &= g(x, y) + \lambda \sum_{j=1}^{N} u_j \int_{\Omega} K(x, y, t, s)\phi_j(t, s)\mathrm{d}t\mathrm{d}s. \end{aligned} \tag{17}$$

Using Eq. (15), Eq. (17) is converted into

$$\sum_{j=1}^{N} \phi_j(x, y)u_j = g(x, y) + \lambda \sum_{j=1}^{N} u_j \int_{\Omega_{\mathbf{x}_j}} K(x, y, t, s)\phi_j(t, s)\mathrm{d}t\mathrm{d}s, \tag{18}$$

where $\Omega_{\mathbf{x}_j}$ is the support domain of $\mathbf{x}_j = (x_j, y_j)$, that is a disk centered at $\mathbf{x}_j$ with radius r_s.

Now, setting $\mathbf{x} = \mathbf{x}_i,\ i = 1, 2, 3, \ldots, N$ (N is the number of total nodes on Ω) in the above equation implies

$$\sum_{j=1}^{N} \phi_j(x_i, y_i)u_j = g(x_i, y_i) + \lambda \sum_{j=1}^{N} u_j \int_{\Omega_{\mathbf{x}_j}} K(x_i, y_i, t, s)\phi_j(t, s)\mathrm{d}t\mathrm{d}s, \tag{19}$$

or equivalently

$$\sum_{j=1}^{N} \left(\delta_{ij} - \lambda \int_{\Omega_{\mathbf{x}_j}} K(x_i, y_i, t, s)\phi_j(t, s)\mathrm{d}t\mathrm{d}s\right) u_j = g(x_i, y_i), \quad i = 1, 2, 3, \ldots, N, \tag{20}$$

because all RPIM shape functions have the Kronecker delta function property, i.e.

$$\phi_j(x_i, y_i) = \delta_{ij} = \begin{cases} 1, & i = j; \\ 0, & i \neq j. \end{cases} \tag{21}$$

The matrix form of Eq. (20) can be given as follows:

$$[\mathbf{I} - \lambda \mathbf{A}]\, U = \mathbf{g}, \tag{22}$$

where $U = (u_1, u_2, \ldots, u_N)^T$ and, $N \times N$ matrix $\mathbf{A}$ and N-vector $\mathbf{g}$ are defined as follows:

$$\mathbf{A}_{ij} = \int_{\Omega_{\mathbf{x}_j}} K(x_i, y_i, t, s)\phi_j(t, s)\mathrm{d}t\mathrm{d}s, \tag{23}$$

$$\mathbf{g}_i = g(x_i, y_i). \tag{24}$$

Moreover, The integral term (23) is evaluated by Gaussian quadrature rule.

4. Convergence analysis and error estimates

In this section, a convergence analysis for our numerical technique to solve Eq. (1) will be provided. The aim is to show that the rate of convergence is exponential, i.e., the spectral accuracy can be obtained for the proposed spectral meshless radial point interpolation (SMRPI) approximation. First, we restrict ourselves to the domains satisfying an interior cone condition defined as follows.

Definition 4.1. A set $\Omega \subset \mathbb{R}^2$ is said to satisfy an interior cone condition if there exist an angle $\theta \in (0, \frac{\pi}{2})$ and a radius $r > 0$ such that for every $\mathbf{x} \in \Omega$ a unit vector $\xi(\mathbf{x})$ exists such that the cone

$$C(\mathbf{x}, \xi(\mathbf{x}), \theta, r) = \left\{\mathbf{x} + \lambda \mathbf{y} : \mathbf{y} \in \mathbb{R}^2, \|\mathbf{y}\|_2 = 1, \mathbf{y}^T \xi(\mathbf{x}) \geq \cos\theta, \lambda \in [0, r]\right\}, \tag{25}$$

is contained in Ω.

Now, we present some definitions which are important to measure the quality of data points and to estimate the rate of convergence in the interpolation by RBFs in the frame work of SMRPI.

Definition 4.2. The fill distance of a set of points $X = \{\mathbf{x}_1, \ldots, \mathbf{x}_N\} \subset \Omega$ for a bounded domain Ω is defined by

$$h_{X,\Omega} = \sup_{\mathbf{x} \in \Omega} \min_{1 \leq j \leq N} \|\mathbf{x} - \mathbf{x}_j\|_2. \tag{26}$$

There is a close connection between the radial basis functions and the reproducing kernels that are defined in the following [51]. All of the strictly positive definite radial basis functions give rise to reproducing kernels with respect to some Hilbert spaces.

Definition 4.3. Let H be a real Hilbert space of functions $u : \Omega \to \mathbb{R}$. A function $K : \Omega \times \Omega \to \mathbb{R}$ is called reproducing kernel for H if

- $K(\mathbf{x}, .) \in H$ for all $x \in \Omega$,
- $u(\mathbf{x}) = \left\langle u, K(., \mathbf{x})\right\rangle_H$ for all $u \in H$ and all $\mathbf{x} \in \Omega$.

If we assume that $K(\mathbf{x}, \mathbf{y}) = \Phi(\mathbf{x} - \mathbf{y})$, $\mathbf{x}, \mathbf{y} \in \mathbb{R}^d$, where Φ is a strictly radial basis function, then it is shown that K is a symmetric reproducing kernel [52] and also

$$H_\Phi(\Omega) = \text{span}\left\{\Phi(\cdot - \mathbf{y}) : \mathbf{y} \in \Omega\right\}, \tag{27}$$

is the pre-Hilbert space with an associated bilinear form

$$\left\langle \sum_{j=1}^{N} c_j \Phi(\cdot - \mathbf{x}_j), \sum_{k=1}^{N} d_k \Phi(\cdot - \mathbf{y}_k)\right\rangle_\Phi = \sum_{j=1}^{N}\sum_{k=1}^{N} c_j d_k \Phi(\mathbf{x}_j, \mathbf{y}_k), \tag{28}$$

provided $\mathbf{x}_j, \mathbf{y}_k \in \Omega$.

Definition 4.4. The native space $\mathscr{H}_\Phi(\Omega)$ of Φ is now defined to be the completion of $H_\Phi(\Omega)$ with respect to the Φ-norm $\|\cdot\|_\Phi$ so that $\|u\|_\Phi = \|u\|_{\mathscr{H}_\Phi(\Omega)}$ for all $u \in \mathscr{H}_\Phi(\Omega)$.

Now, we give the following four important lemmas which play essential role in our error analysis, the first one is about the error of Gaussian quadrature rule in integrating (23).

Lemma 4.5 (*[53], Integration Error from Gaussian Quadrature*). *Assume that a $(M+1)$-point Gaussian quadrature formula is used to integrate the product $u(\mathbf{x})\phi(\mathbf{x})$, where $u \in H^m(\Omega)$ (Sobolev space of order m) for some $m \geq 1$ and $\phi \in \mathscr{H}_\Phi(\Omega)$. Then there exists a constant C independent of M such that*

$$\left| \int_\Omega u(\mathbf{x})\phi(\mathbf{x})d\mathbf{x} - (u,\phi)_M \right| \leq CM^{-m}\|u\|_{H^m(\Omega)}\|\phi\|_{L^2(\Omega)}, \tag{29}$$

where

$$\|u\|_{H^m(\Omega)} = \left(\sum_{|\alpha|\leq m} \|D^\alpha u\|^2_{L^2(\Omega)} \right)^{\frac{1}{2}}, \tag{30}$$

$$(u,\phi)_M = \sum_{j=0}^{M} \omega_j u(\mathbf{x}_j)\phi(\mathbf{x}_j), \tag{31}$$

$$H^m(\Omega) = \left\{ \begin{matrix} u \in L^2(\Omega) : \text{ for each nonnegative multi-index } \alpha \text{ with } |\alpha| \\ \leq m, \text{ the distributional derivative } D^\alpha u \text{ belongs to } L^2(\Omega) \end{matrix} \right\}. \tag{32}$$

The following lemma is about the error bound for approximating u by $I_N u = \sum_{j=1}^N \phi_j(\mathbf{x})u_j$, defined in (14), where $\phi_j(\mathbf{x})$ is shape function defined by (10). Notice that $I_N u$ could be equivalently rewritten as $I_N u = \sum_{j=1}^N a_j R_j(\mathbf{x})$, where $R_j(\mathbf{x})$ is strictly positive definite function.

Lemma 4.6 (*[52]*). *Let $\Omega \subset \mathbb{R}^2$ be open and bounded, satisfying an interior cone condition. Suppose that Φ is IQ or IMQ radial basis function and $I_N u$ approximation to $u \in \mathscr{H}_\Phi(\Omega)$. Then there exist constants, $c > 0$ such that the following estimates hold:*

$$\|u - I_N u\|_{L^\infty(\Omega)} \leq C\|u\|_{\mathscr{H}_\Phi(\Omega)}, \quad C = \begin{cases} e^{-\frac{c|\log h_{X,\Omega}|}{h_{X,\Omega}}}, & \Phi \text{ is GA;} \\ e^{-\frac{c}{h_{X,\Omega}}}, & \Phi \text{ is IQ or IMQ.} \end{cases} \tag{33}$$

Lemma 4.7 (*[52]*). *Let $\Omega \subset \mathbb{R}^2$ be open and bounded, satisfying an interior cone condition. Suppose that Φ is strictly positive definite and $I_N u$ approximation to $u \in H^m(\Omega)$. Then there exist constants, $C > 0$ such that the following estimates hold:*

$$\|u - I_N u\|_{L^2(\Omega)} \leq Ch^{\frac{m}{2}}_{X,\Omega}\|u\|_{H^m(\Omega)}. \tag{34}$$

Lemma 4.8 (*[52]*). *Let $\Omega \subset \mathbb{R}^2$ be open and bounded, satisfying an interior cone condition. Suppose that Φ is strictly positive definite and $I_N u$ approximation to $u \in H^m(\Omega)$. Then there exist constants, $C > 0$ such that the following estimates hold:*

$$\|u - I_N u\|_{H^m(\Omega)} \leq Ch^{\tau-m}_{X,\Omega}\|u\|_{H^m(\Omega)}, \quad \tau > 1. \tag{35}$$

Lemma 4.9 (*Gronwall Inequality*). *If a non-negative integrable function $E(\mathbf{x})$ satisfies*

$$E(\mathbf{x}) = C_1 \int_\Omega E(\mathbf{x})d\mathbf{x} + G(\mathbf{x}), \tag{36}$$

where $G(\mathbf{x})$ is an integrable function, then

$$\|E\|_{L^p(\Omega)} \leq C\|G\|_{L^p(\Omega)}, \quad p \geq 1. \tag{37}$$

Now, we will carry our convergence analysis in both L^2 and L^∞ spaces.

4.1. Error analysis in L^2

Theorem 4.10. *Let u be the exact solution of the Fredholm equation (1) and assume that*

$$U^N(\mathbf{x}) = \sum_{j=1}^{N} u_j\phi_j(\mathbf{x}), \tag{38}$$

where u_j is given by (22) and $\phi_j(\mathbf{x})$ is the jth shape function defined by (10) associated with the $X = \{\mathbf{x}_1, \ldots, \mathbf{x}_N\} \subset \Omega$ covering the domain Ω. If $u \in H^m(\Omega)$, $m \geq 1$, and $u \in \mathscr{H}_\Phi(\Omega)$, then

$$\|u - U^N\|_{L^2(\Omega)} \leq CM^{-m} \max_{\mathbf{x}\in\Omega} \|K(\mathbf{x}, \cdot)\|_{H^m(\Omega)} \|u\|_{L^2(\Omega)} + C\sqrt{h_{X,\Omega}}\|u\|_{H^m(\Omega)}, \tag{39}$$

provided that M is sufficiently large and $h_{X,\Omega}$ is sufficiently small, where C is a constant independent of M and N.

Proof. Following the notations of (31), we let

$$(K(\mathbf{x}, \mathbf{s}), \phi(\mathbf{s}))_{M,\mathbf{s}} = \sum_{j=0}^{M} \omega_j K(\mathbf{x}, \mathbf{s}_j)\phi(\mathbf{s}_j). \tag{40}$$

Then the numerical scheme (19) can be written as

$$u_i - \lambda \sum_{j=1}^{N} u_j \left(\sum_{k=0}^{M} \omega_k K(\mathbf{x}_i, \mathbf{s}_k)\phi_j(\mathbf{s}_k) \right) = g(\mathbf{x}_i), \tag{41}$$

or equivalently

$$u_i - \lambda \left(K(\mathbf{x}_i, \mathbf{s}), U^N(\mathbf{s})\right)_{M,\mathbf{s}} = g(\mathbf{x}_i), \tag{42}$$

which gives

$$u_i - \lambda \int_\Omega K(\mathbf{x}_i, \mathbf{s})U^N(\mathbf{s})\mathrm{d}\mathbf{s} = g(\mathbf{x}_i) + J_1(\mathbf{x}_i), \quad 1 \leq i \leq N, \tag{43}$$

where

$$J_1(\mathbf{x}) = \lambda \left(K(\mathbf{x}, \mathbf{s}), U^N(\mathbf{s})\right)_{M,\mathbf{s}} - \lambda \int_\Omega K(\mathbf{x}, \mathbf{s})U^N(\mathbf{s})\mathrm{d}\mathbf{s}. \tag{44}$$

Using Lemma 4.5 gives

$$|J_1(\mathbf{x})| \leq C_1 M^{-m} \|K(\mathbf{x}, \cdot)\|_{H^m(\Omega)} \|U^N\|_{L^2(\Omega)}. \tag{45}$$

Considering (43) and multiplying $\phi_i(\mathbf{x})$ on both sides and summing up from 0 to N yields

$$U^N(\mathbf{x}) - \lambda I_N \left(\int_\Omega K(\mathbf{x}, \mathbf{s})u(\mathbf{s})\mathrm{d}\mathbf{s} \right) - \lambda I_N \left(\int_\Omega K(\mathbf{x}, \mathbf{s})e(\mathbf{s})\mathrm{d}\mathbf{s} \right) = I_N(g) + I_N(J_1), \tag{46}$$

where U^N is defined by (38), the interpolation operator I_N is defined in paragraph after Lemma 4.5, e denotes the error function, i.e.,

$$e(\mathbf{x}) = U^N(\mathbf{x}) - u(\mathbf{x}), \quad \mathbf{x} \in \Omega. \tag{47}$$

It follows from (46) and (1) that

$$U^N(\mathbf{x}) + I_N(g - u) - \lambda I_N \left(\int_\Omega K(\mathbf{x}, \mathbf{s})e(\mathbf{s})\mathrm{d}\mathbf{s} \right) = I_N(g) + I_N(J_1), \tag{48}$$

which gives

$$e(\mathbf{x}) + (u - I_N u)(\mathbf{x}) - \lambda I_N \left(\int_\Omega K(\mathbf{x}, \mathbf{s})e(\mathbf{s})\mathrm{d}\mathbf{s} \right) = I_N(J_1). \tag{49}$$

Consequently,

$$e(\mathbf{x}) - \lambda \int_\Omega K(\mathbf{x}, \mathbf{s})e(\mathbf{s})\mathrm{d}\mathbf{s} = I_N(J_1) + J_2(\mathbf{x}) + J_3(\mathbf{x}), \tag{50}$$

where

$$J_2 = I_N u(\mathbf{x}) - u(\mathbf{x}), \qquad J_3 = \lambda I_N \left(\int_\Omega K(\mathbf{x}, \mathbf{s})e(\mathbf{s})\mathrm{d}\mathbf{s} \right) - \lambda \int_\Omega K(\mathbf{x}, \mathbf{s})e(\mathbf{s})\mathrm{d}\mathbf{s}. \tag{51}$$

It follows from the Gronwall inequality (see Lemma 4.9) with $p = 2$ that

$$\|e\|_{L^2(\Omega)} \leq C \left(\|I_N(J_1)\|_{L^2(\Omega)} + \|J_2\|_{L^2(\Omega)} + \|J_3\|_{L^2(\Omega)} \right). \tag{52}$$

Using (45) and (13) gives

$$\begin{aligned}\|I_N(J_1)\|_{L^2(\Omega)} &\le C_1 M^{-m} \max_{\mathbf{x}\in\Omega} \|K(\mathbf{x},\cdot)\|_{H^m(\Omega)} \|U^N\|_{L^2(\Omega)} \\ &\le C_1 M^{-m} \max_{\mathbf{x}\in\Omega} \|K(\mathbf{x},\cdot)\|_{H^m(\Omega)} (\|e\|_{L^2(\Omega)} + \|u\|_{L^2(\Omega)}). \end{aligned} \tag{53}$$

Using the L^2-error bound for the SMRPI approximation (i.e., Lemma 4.7) gives

$$\|J_2\|_{L^2(\Omega)} \le C_2 \sqrt{h_{X,\Omega}} \|u\|_{H^m(\Omega)} \tag{54}$$

and, by letting $m = 1$ in Lemma 4.7, yields

$$\|J_3\|_{L^2(\Omega)} \le \lambda C_3 \sqrt{h_{X,\Omega}} \left\| \int_\Omega \mathrm{D}[K(\mathbf{x},\mathbf{s})] e(\mathbf{s}) \mathrm{d}\mathbf{s} \right\|_{L^2(\Omega)}, \tag{55}$$

where, D is the distributional derivatives with respect to $\mathbf{x}$ which is bounded by D_1 from (32), then (55) yields

$$\|J_3\|_{L^2(\Omega)} \le \lambda C_3 D_1 \sqrt{h_{X,\Omega}} \|e\|_{L^2(\Omega)}. \tag{56}$$

The above estimates, together with (52), yield

$$\begin{aligned}\|e\|_{L^2(\Omega)} &\le C C_1 M^{-m} \max_{\mathbf{x}\in\Omega} \|K(\mathbf{x},\cdot)\|_{H^m(\Omega)} (\|e\|_{L^2(\Omega)} + \|u\|_{L^2(\Omega)}) \\ &\quad + C C_2 \sqrt{h_{X,\Omega}} \|u\|_{H^m(\Omega)} + \lambda C C_3 D_1 \sqrt{h_{X,\Omega}} \|e\|_{L^2(\Omega)}, \end{aligned} \tag{57}$$

which leads to (39) provided that M is sufficiently large and $h_{X,\Omega}$ is sufficiently small. This completes the proof of this theorem.

4.2. Error analysis in L^∞

Below we will extend the L^2 error estimate in the last subsection to the L^∞ space.

Theorem 4.11. *Let u be the exact solution of the Fredholm equation (1) and U^N be defined by (38). If $u \in H^m(\Omega)$ and $u \in \mathscr{H}_\Phi(\Omega)$, then for $m \ge 1$,*

$$\|u - U^N\|_{L^2(\Omega)} \le C M^{-m} \max_{\mathbf{x}\in\Omega} \|K(\mathbf{x},\cdot)\|_{H^m(\Omega)} \|u\|_{L^2(\Omega)} + C \|u\|_{\mathscr{H}_\Phi(\Omega)}, \tag{58}$$

provided that M is sufficiently large and $h_{X,\Omega}$ is sufficiently small, where C is a constant independent of M and N.

Proof. Following the same procedure as in the proof of Theorem 4.10, we have

$$e(\mathbf{x}) - \lambda \int_\Omega K(\mathbf{x},\mathbf{s}) e(\mathbf{s}) \mathrm{d}\mathbf{s} = I_N(J_1) + J_2(\mathbf{x}) + J_3(\mathbf{x}), \tag{59}$$

where $I_N(J_1)$, J_2 and J_3 are defined by (44) and (51), respectively. It follows from the Gronwall inequality (see Lemma 4.9) that

$$\|e\|_{L^\infty(\Omega)} \le C \left(\|I_N(J_1)\|_{L^\infty(\Omega)} + \|J_2\|_{L^\infty(\Omega)} + \|J_3\|_{L^\infty(\Omega)} \right). \tag{60}$$

Using (45) and (13) gives

$$\begin{aligned}\|I_N(J_1)\|_{L^\infty(\Omega)} &\le C_1 M^{-m} \max_{\mathbf{x}\in\Omega} \|K(\mathbf{x},\cdot)\|_{H^m(\Omega)} \|U^N\|_{L^2(\Omega)} \\ &\le C_1 M^{-m} \max_{\mathbf{x}\in\Omega} \|K(\mathbf{x},\cdot)\|_{H^m(\Omega)} (\|e\|_{L^2(\Omega)} + \|u\|_{L^2(\Omega)}) \\ &\le C_1^* M^{-m} \max_{\mathbf{x}\in\Omega} \|K(\mathbf{x},\cdot)\|_{H^m(\Omega)} (\|e\|_{L^\infty(\Omega)} + \|u\|_{L^2(\Omega)}). \end{aligned} \tag{61}$$

Using Lemma 4.6, we have

$$\|J_2\|_{L^\infty(\Omega)} = \|u - I_N u\|_{L^\infty(\Omega)} \le C_2 \|u\|_{\mathscr{H}_\Phi(\Omega)}. \tag{62}$$

Also, letting $m = 1$ in Lemma 4.7, yields

$$\|J_3\|_{L^2(\Omega)} \le \lambda C_3 \sqrt{h_{X,\Omega}} \left\| \int_\Omega \mathrm{D}[K(\mathbf{x},\mathbf{s})] e(\mathbf{s}) \mathrm{d}\mathbf{s} \right\|_{L^2(\Omega)}, \tag{63}$$

where, D is the distributional derivatives with respect to $\mathbf{x}$ which is bounded by D_1 from (32), then (63) yields

$$\|J_3\|_{L^2(\Omega)} \le \lambda C_3 D_1 \sqrt{h_{X,\Omega}} \|e\|_{L^2(\Omega)} \le C_3^* \sqrt{h_{X,\Omega}} \|e\|_{L^\infty(\Omega)}. \tag{64}$$

On the other hand, considering (30), (35) and (51) with $m = 1$ yields

$$\begin{aligned}\|J_3\|_{H^1(\Omega)} &\leq \lambda C_3^{\star} h_{X,\Omega}^{\tau-1} \left\| \int_{\Omega} \mathrm{D}[K(\mathbf{x},\mathbf{s})] e(\mathbf{s}) \mathrm{d}\mathbf{s} \right\|_{L^2(\Omega)} \\ &\leq \lambda D_1 C_3^{\star} h_{X,\Omega}^{\tau-1} \|e\|_{L^2(\Omega)} \\ &\leq \lambda D_1 C_3^{\star\star} h_{X,\Omega}^{\tau-1} \|e\|_{L^\infty(\Omega)}, \quad \tau > 1. \end{aligned} \tag{65}$$

Using the inequality in the Sobolev Space [53]

$$\|\omega\|_{L^\infty(\Omega)} \leq c \|\omega\|_{L^2(\Omega)}^{\frac{1}{2}} \|\omega\|_{H^1(\Omega)}^{\frac{1}{2}}, \tag{66}$$

we have

$$\|J_3\|_{L^\infty(\Omega)} \leq C_3^{\dagger} h_{X,\Omega}^{\frac{2\tau-1}{4}} \|e\|_{L^\infty(\Omega)}, \quad \tau > 1. \tag{67}$$

Now, setting estimates (61), (62) and (67) into (60), yields

$$\|e\|_{L^\infty(\Omega)} \leq C C_1^{*} M^{-m} \max_{\mathbf{x}\in\Omega} \|K(\mathbf{x},\cdot)\|_{H^m(\Omega)} (\|e\|_{L^\infty(\Omega)} + \|u\|_{L^2(\Omega)}) + C C_2 \|u\|_{\mathscr{H}_\Phi(\Omega)} + C C_3^{\dagger} h_{X,\Omega}^{\frac{2\tau-1}{4}} \|e\|_{L^\infty(\Omega)}, \tag{68}$$

which leads to (58) provided that M is sufficiently large and $h_{X,\Omega}$ is sufficiently small. This completes the proof of this theorem.

5. Numerical experiments and comparison

In this section, we show the results obtained for three examples using the SMRPI method described in previous sections. To show the accuracy and convergence of the method two kinds of error measures, maximum absolute error $\|u\|_\infty$ and relative error $\|u\|_R$:

$$\|u\|_\infty = \left\| u_{exact} - u_{approx} \right\|_\infty = \max \left\{ |u_{exact}(\mathbf{x}_i) - u_{approx}(\mathbf{x}_i)|,\ i = 1, 2, \ldots, N \right\}, \tag{69}$$

$$\|u\|_R = \sqrt{\frac{\sum_{i=1}^{N} \left(u_{exact}(\mathbf{x}_i) - u_{approx}(\mathbf{x}_i)\right)^2}{\sum_{i=1}^{N} \left(u_{exact}(\mathbf{x}_i)\right)^2}}, \tag{70}$$

are used, where $u_{exact}(\mathbf{x}_i)$ and $u_{approx}(\mathbf{x}_i)$ denote the exact and approximate solutions, respectively. In these examples, N, the number of total nodal points covering Ω, is regularly distributed. Also in order to implement the SMRPI method, the radius of support domain (that is a disk) to construct basis functions is chosen $r_s = h$ (for simplicity), where h is the distance between the nodes in x or y direction. Also, the integrals (23) are evaluated with $16 = 4 \times 4$ points Gaussian quadrature rule.

Example 1. For the first test problem consider Eq. (1) with the following

$$g(x, y) = \frac{1}{(1 + x + y)^2} - \frac{x}{6(8 + y)}, \tag{71}$$

$$K(x, y, t, s) = \frac{x}{(8 + y)(1 + t + s)}, \qquad \lambda = 1, \tag{72}$$

$$\Omega = [0, 1] \times [0, 1]. \tag{73}$$

In this example the domain is supposed to be regular and the exact solution is

$$u(x, y) = \frac{1}{(1 + x + y)^2}. \tag{74}$$

Here, the presented technique is employed to solve the problem. The maximum absolute error ($\|u\|_\infty$) of SMRPI solution with number of nodal points $N = 1681$ and different strictly positive definite RBFs are given in Table 2. Also, Fig. 2 shows the maximum absolute and relative error for different number of nodal points and different strictly positive definite RBFs.

Table 2
Maximum absolute error ($\|u\|_\infty$) of SMRPI solution with $N = 1681$ and different RBFs for Example 1.

x	y	GA	IMQ	IQ
0.0	0.0	0.000000e+000	0.000000e+000	0.000000e+000
0.1	0.1	5.314645e−005	5.291803e−005	5.325470e−005
0.2	0.2	1.049967e−004	1.045454e−004	1.052105e−004
0.3	0.3	1.555974e−004	1.549287e−004	1.559144e−004
0.4	0.4	2.049935e−004	2.041124e−004	2.054110e−004
0.5	0.5	2.532272e−004	2.521388e−004	2.537430e−004
0.6	0.6	3.003393e−004	2.990484e−004	3.009510e−004
0.7	0.7	3.463683e−004	3.448796e−004	3.470737e−004
0.8	0.8	3.913512e−004	3.896691e−004	3.921482e−004
0.9	0.9	4.353232e−004	4.334522e−004	4.362098e−004
1.0	1.0	4.783181e−004	4.762623e−004	4.792923e−004

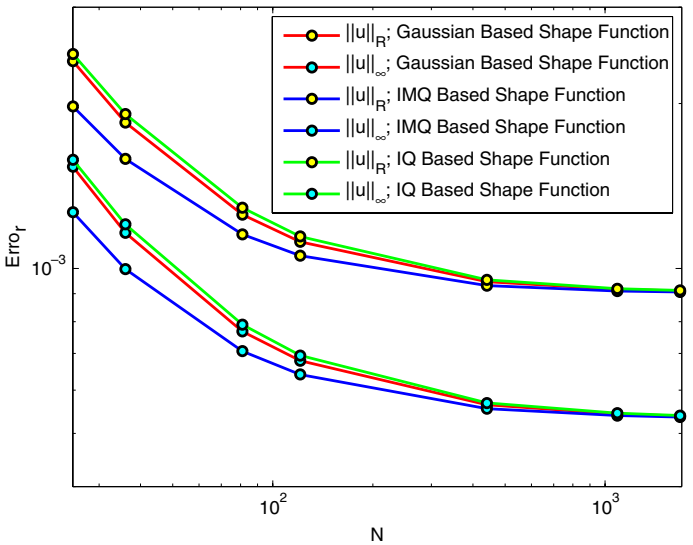

Fig. 2. The maximum absolute and relative error versus number of nodal points for Example 1.

Example 2. As a second test problem, we consider Eq. (1) with

$$g(x,y) = x^2 + y^2 - \frac{98 - 36e}{3e} e^{-(x+y)}, \tag{75}$$

$$K(x,y,t,s) = e^{-(x+y+t+s)}(1 - t - s), \qquad \lambda = 1, \tag{76}$$

$$\Omega = \{(x,y) : 0 \le x + y \le 1, 0 \le x \le 1\}. \tag{77}$$

The exact solution is

$$u(x,y) = x^2 + y^2. \tag{78}$$

In this example, the domain is chosen to be general. Fig. 3 shows the domain for different number of nodal points. As previous example, we apply SMRPI to solve this problem. The maximum absolute error ($\|u\|_\infty$) of SMRPI solution with number of nodal points $N = 1326$ and different strictly positive definite RBFs are given in Table 3. Also, Fig. 4 shows the maximum absolute error of SMRPI solution with inverse quadratic RBF and number of nodal points $N = 1326$.

Example 3. As a last test problem, let us consider Eq. (1) with

$$g(x,y) = \left(x - \frac{1}{2}\right)^2 + \left(y - \frac{1}{2}\right)^2 - \frac{1}{20480(x+y)}, \tag{79}$$

$$K(x,y,t,s) = \frac{s}{100\pi(x+y)}, \qquad \lambda = 1, \tag{80}$$

$$\Omega = \left\{(x,y) : \left(x - \frac{1}{2}\right)^2 + 4\left(y - \frac{1}{2}\right)^2 \le \frac{1}{4}\right\}. \tag{81}$$

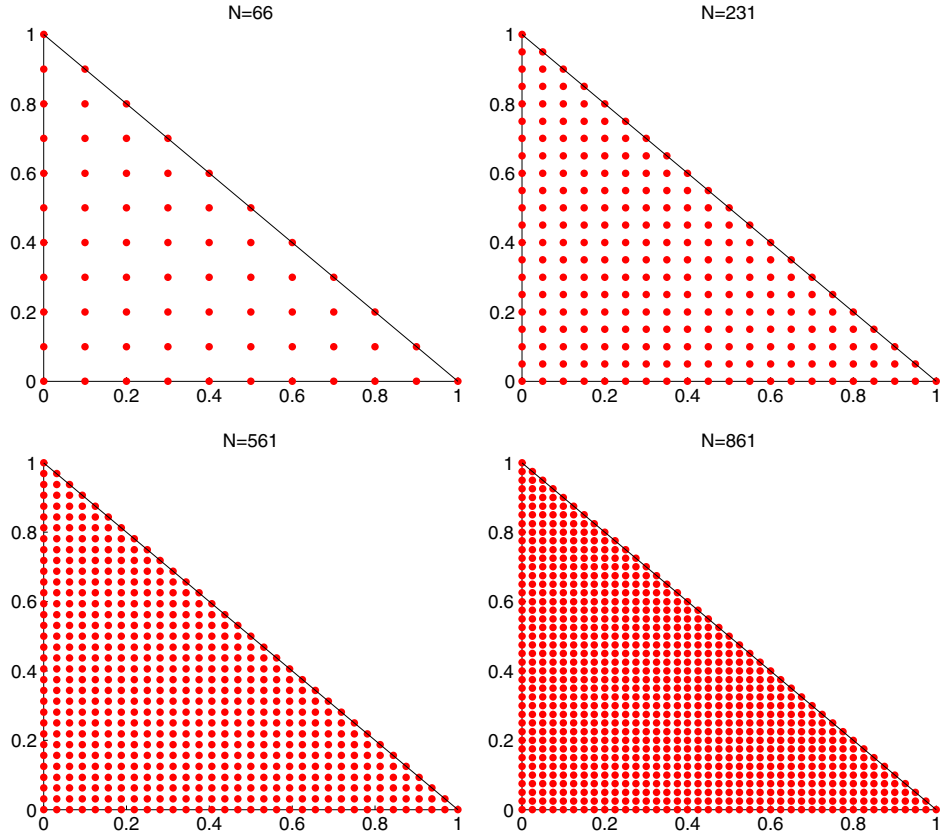

Fig. 3. The domain of Example 2 with different number of nodal points.

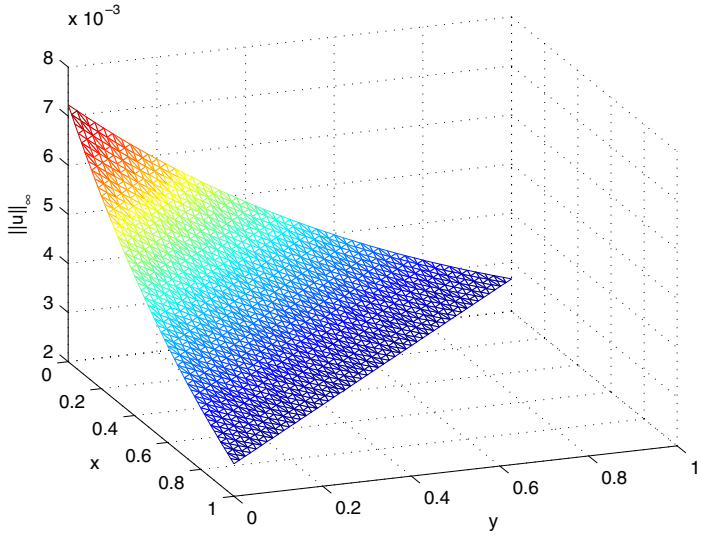

Fig. 4. The maximum absolute error of SMRPI solution with $N = 1326$ and inverse quadratic RBF for Example 2.

The exact solution is

$$u(x, y) = \left(x - \frac{1}{2}\right)^2 + \left(y - \frac{1}{2}\right)^2. \tag{82}$$

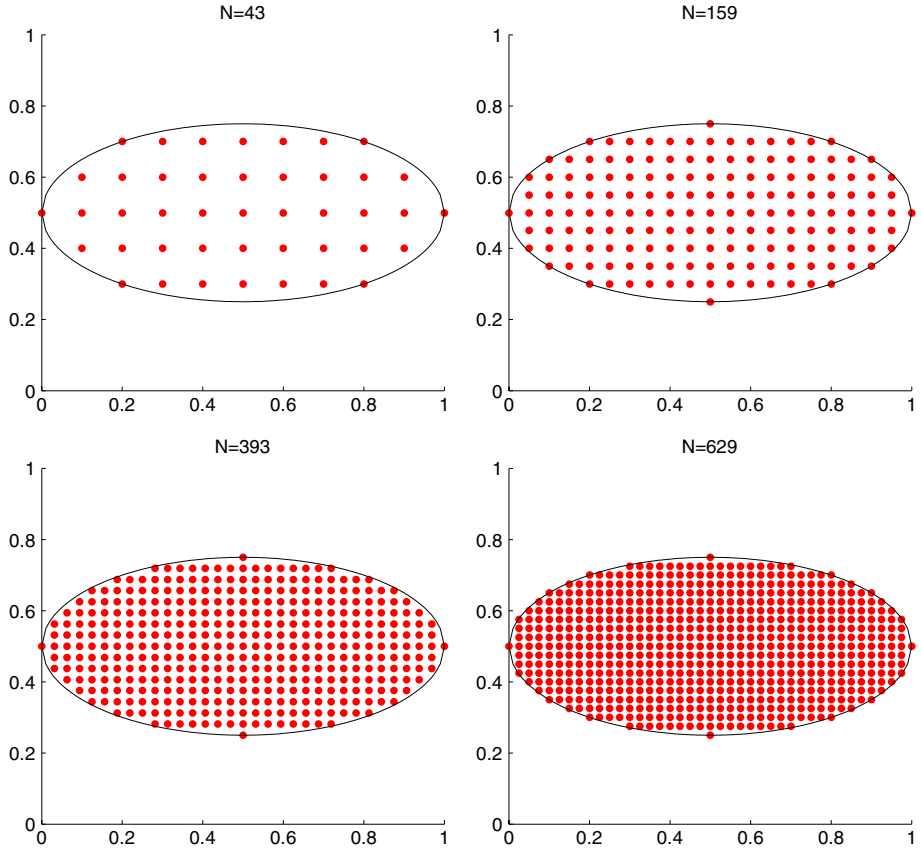

Fig. 5. The domain of Example 3 with different number of nodal points.

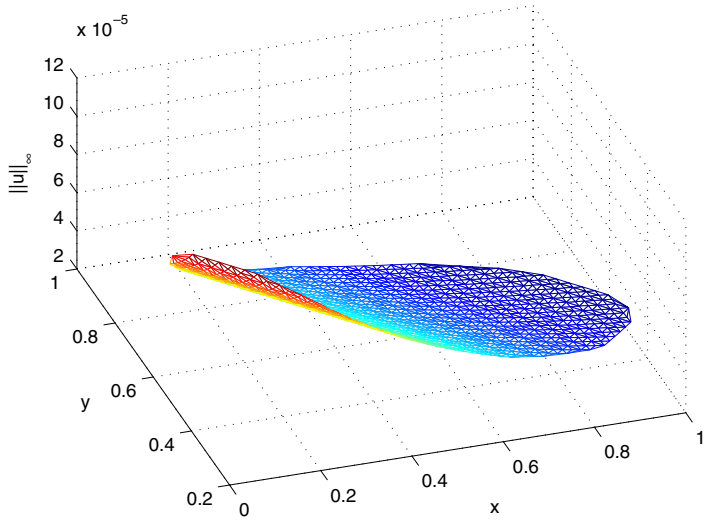

Fig. 6. The maximum absolute error of SMRPI solution with $N = 629$ and inverse multiquadratic RBF for Example 3.

As it is seen, the domain is the inside of an oval. Fig. 5 shows the domain for different number of nodal points. Furthermore, the maximum absolute error of SMRPI solution by inverse multiquadratic RBF and number of nodal points $N = 629$ has been plotted in Fig. 6.

Table 3
Maximum absolute error ($\|u\|_\infty$) of SMRPI solution with $N = 1326$ and different RBFs for Example 2.

x	y	GA	IMQ	IQ
0.0	0.0	7.233361e−003	7.233412e−003	7.233361e−003
0.1	0.1	5.922175e−003	5.922217e−003	5.922175e−003
0.2	0.2	4.848667e−003	4.848701e−003	4.848667e−003
0.3	0.3	3.969753e−003	3.969780e−003	3.969753e−003
0.4	0.4	3.250159e−003	3.250181e−003	3.250159e−003
0.5	0.5	2.661005e−003	2.661023e−003	2.661005e−003

6. Conclusions

In this paper, a new spectral meshless radial point interpolation (SMRPI) method has been proposed and applied to the two-dimensional Fredholm integral equations of the second kind on general domains. The present method is based on meshless methods and benefits from spectral collocation techniques. The interpolation with the help of strictly positive definite radial basis functions has been used to construct shape (basis) functions which have Kronecker delta function property. The method does not need any domain element and so it is independent of the geometry of the domain. We have given error analysis with some numerical experiments to show the validity and efficiency of SMRPI.

References

[1] P. Assari, H. Adibi, M. Dehghan, A meshless method for solving nonlinear two-dimensional integral equations of the second kind on non-rectangular domains using radial basis functions with error analysis, J. Comput. Appl. Math. 239 (2013) 72–92.
[2] J. Bremer, V. Rokhlin, I. Sammis, Universal quadratures for boundary integral equations on two-dimensional domains with corners, J. Comput. Phys. 229 (2010) 8259–8280.
[3] X. Li, E. Rong, Solution of a class of two-dimensional integral equations, J. Comput. Appl. Math. 145 (2002) 335–343.
[4] P. Anselone, Collectively Compact Operator Approximation Theory, Prentice-Hall, Englewood Cliffs, NJ, 1971.
[5] K. Atkinson, A Survey of Numerical Methods for the Solution of Fredholm Integral Equations of the Second Kind, SIAM, Philadelphia, PA, 1976.
[6] K. Atkinson, The Numerical Solution of Integral Equations of the Second Kind, Cambridge University Press, Cambridge, 1997.
[7] C. Baker, The Numerical Treatment of Integral Equations, Clarendon Press, Oxford, 1977.
[8] L. Delves, J. Mohamed, Computational Methods for Integral Equations, Cambridge University Press, New York, 1985.
[9] B. Alpert, G. Beylkin, R. Coifman, V. Rokhlin, Wavelets for the fast solution of second-kind integral equations, SIAM J. Sci. Comput. 14 (1993) 159–184.
[10] G. Han, R. Wang, Richardson extrapolation of iterated discrete Galerkin solution for two-dimensional Fredholm integral equations, Comput. Appl. Math. 139 (2002) 49–63.
[11] M. Hadizadeh, M. Asgary, An efficient numerical approximation for the linear class of mixed integral equations, Appl. Math. Comput. 167 (2005) 1090–1100.
[12] A. Alipanah, M. Dehghan, Numerical solution of the nonlinear Fredholm integral equations by positive definite functions, Appl. Math. Comput. 190 (2007) 1754–1761.
[13] A. Golbabai, S. Seifollahi, Numerical solution of the second kind integral equations using radial basis function networks, Appl. Math. Comput. 174 (2006) 877–883.
[14] A. Golbabai, S. Seifollahi, Radial basis function networks in the numerical solution of linear integro-differential equations, Appl. Math. Comput. 188 (2007) 427–432.
[15] K. Parand, J. Rad, Numerical solution of nonlinear Volterra–Fredholm–Hammerstein integral equations via collocation method based on radial basis functions, Appl. Math. Comput. 218 (2012) 5292–5309.
[16] A. Golbabai, M. Mammadov, S. Seifollahi, Solving a system of nonlinear integral equations by an RBF network, Comput. Math. Appl. 57 (2009) 1651–1658.
[17] A. Alipanah, S. Esmaeili, Numerical solution of the two-dimensional Fredholm integral equations using Gaussian radial basis function, J. Comput. Appl. Math. 235 (2011) 5342–5347.
[18] D. Mirzaei, M. Dehghan, A meshless based method for solution of integral equations, Appl. Numer. Math. 60 (2010) 245–262.
[19] G. Liu, Y. Gu, An Introduction to Meshfree Methods and their Programing, Springer, 2005.
[20] S. Atluri, The Meshless Method (MLPG) for Domain and BIE Discretizations, Tech. Science Press, 2004.
[21] S. Atluri, S. Shen, The Meshless Local Petrov-Galerkin (MLPG) Method, Tech. Science Press, 2002.
[22] T. Belytschko, Y.Y. Lu, L. Gu, Element-free Galerkin methods, Internat. J. Numer. Methods Engrg. 37 (2) (1994) 229–256.
[23] T. Belytschko, Y.Y. Lu, L. Gu, Element free Galerkin methods for static and dynamic fracture, Int. J. Solids Struct. 32 (1995) 2547–2570.
[24] Y. Duan, Y. Tan, A meshless Galerkin method for Dirichlet problems using radial basis functions, J. Comput. Appl. Math. 196 (2) (2006) 394–401.
[25] P. Assari, H. Adibi, M. Dehghan, A meshless discrete Galerkin (MDG) method for the numerical solution of integral equations with logarithmic kernels, J. Comput. Appl. Math. 267 (2014) 160–181.
[26] R.S.M. Dehghan, A meshless local Petrov–Galerkin method for the time-dependent Maxwell equations, J. Comput. Appl. Math. 268 (2014) 93–110.
[27] D. Mirzaei, M. Dehghan, Meshless local Petrov–Galerkin (MLPG) approximation to the two dimensional sine-Gordon equation, J. Comput. Appl. Math. 233 (10) (2010) 2737–2754.
[28] A. Fili, A. Naji, Y. Duan, Coupling three-field formulation and meshless mixed Galerkin methods using radial basis functions, J. Comput. Appl. Math. 234 (8) (2010) 2456–2468.
[29] M. Peng, D. Li, Y. Cheng, The complex variable element-free Galerkin (CVEFG) method for elasto-plasticity problems, Eng. Struct. 33 (1) (2011) 127–135.
[30] B. Dai, Y. Cheng, An improved local boundary integral equation method for two-dimensional potential problems, Int. J. Appl. Mech. 2 (2) (2010) 421–436.
[31] F. Bai, D. Li, J. Wang, Y. Cheng, An improved complex variable element-free Galerkin method for two-dimensional elasticity problems, Chin. Phys. B 21 (2) (2012) 020204–1–10.
[32] S. Atluri, S. Shen, The meshless local Petrov–Galerkin (MLPG) method: a simple and less costly alternative to the finite element and boundary element methods, Comput. Modeling Eng. Sci. 3 (2002) 11–51.
[33] E. Kansa, Multiquadrics-a scattered data approximation scheme with applications to computational fluid-dynamics. I. Surface approximations and partial derivative estimates, Comput. Math. Appl. 19 (8–9) (1990) 127–145.
[34] M. Dehghan, A. Shokri, A numerical method for solution of the two dimensional sine-Gordon equation using the radial basis functions, Math. Comput. Simul. 79 (2008) 700–715.

[35] S. Jakobsson, B. Andersson, F. Edelvik, Rational radial basis function interpolation with applications to antenna design, J. Comput. Appl. Math. 233 (4) (2009) 889–904.
[36] Y. Zhang, Y. Tan, Meshless schemes for unsteady Navier–Stokes equations in vorticity formulation using radial basis functions, J. Comput. Appl. Math. 192 (2) (2006) 328–338.
[37] S. Abbasbandy, H.R. Ghehsareh, I. Hashim, A meshfree method for the solution of two-dimensional cubic nonlinear schrödinger equation, Eng. Anal. Bound. Elem. 37 (6) (2013) 885–898.
[38] S. Abbasbandy, H.R. Ghehsareh, I. Hashim, Numerical analysis of a mathematical model for capillary formation in tumor angiogenesis using a meshfree method based on the radial basis function, Eng. Anal. Bound. Elem. 36 (12) (2012) 1811–1818.
[39] E. Shivanian, Analysis of meshless local radial point interpolation (MLRPI) on a nonlinear partial integro-differential equation arising in population dynamics, Eng. Anal. Bound. Elem. 37 (2013) 1693–1702.
[40] E. Shivanian, Meshless local Petrov–Galerkin (MLPG) method for three-dimensional nonlinear wavee quations via moving leasts quares approximation, Eng. Anal. Bound. Elem. 50 (2015) 249–257.
[41] A. Shirzadi, L. Ling, S. Abbasbandy, Meshless simulations of the two-dimensional fractional-time convection–diffusion–reaction equations, Eng. Anal. Bound. Elem. 36 (2012) 1522–1527.
[42] M. Dehghan, A. Ghesmati, Numerical simulation of two-dimensional sine-gordon solitons via a local weak meshless technique based on the radial point interpolation method (RPIM), Comput. Phys. Comm. 181 (2010) 772–786.
[43] L. Trefethen, Spectral methods in MATLAB, SIAM, PA, Philadelphia, 2000.
[44] S. Abbasbandy, E. Shivanian, Multiple solutions of mixed convection in a porous medium on semi-infinite interval using pseudo-spectral collocation method, Commun. Nonlinear Sci. Numer. Simul. 16 (2011) 2745–2752.
[45] T. Tang, On spectral methods for Volterra integral equations and the convergence analysis, J. Comput. Math. 26 (6) (2008) 825–837.
[46] E. Shivanian, Analysis of meshless local and spectral meshless radial point interpolation (MLRPI and SMRPI) on 3-d nonlinear wave equations, Ocean Eng. 89 (2014) 173–188.
[47] E. Shivanian, A new spectral meshless radial point interpolation (SMRPI) method: A well-behaved alternative to the meshless weak forms, Eng. Anal. Bound. Elem. 54 (2015) 1–12.
[48] W. Cheney, W. Light, A Course in Approximation Theory, William Allan, New York, 1999.
[49] C. Franke, R. Schaback, Solving partial differential equations by collocation using radial basis functions, Appl. Math. Comput. 93 (1997) 73–82.
[50] M. Sharan, E. Kansa, S. Gupta, Application of the multiquadric method for numerical solution of elliptic partial differential equations, Appl. Math. Comput. 84 (1997) 275–302.
[51] M. Buhmann, Radial Basis Functions: Theory and Implementations, Cambridge University Press, Cambridge, 2003.
[52] H. Wendland, Scattered Data Approximation, Cambridge University Press, Cambridge, 2005.
[53] C. Canuto, M. Hussaini, A. Quarteroni, T. Zang, Spectral Methods: Fundamentals in Single Domains, Springer-Verlag, Berlin, 2006.